Biotecnia
ISSN: 1665-1456
Universidad de Sonora, División de Ciencias Biológicas y de la Salud

Arroyo-Loranca, Raquel Gabriela; Rivera-Perez, Crisalejandra; Hernandez-Adame, Luis; Cruz Villacorta, Ariel Arturo; Rodriguez-Lopez, Jose Luis; Hernandez-Saavedra, Norma Yolanda

Effect of ion and protein concentration of Ps19, a shell protein from *Pteria sterna, on calcium carbonate polymorph*

Biotecnia, vol. 25, no. 2, 2023, May-August, pp. 136-145
Universidad de Sonora, División de Ciencias Biológicas y de la Salud

DOI: https://doi.org/10.18633/biotecnia.v25i2.1885

Available in: https://www.redalyc.org/articulo.oa?id=672975613016

Biotecnia
Journal of biological and health sciences
http://biotecnia.unison.mx
Universidad de Sonora
ISSN: 1665-1456

Effect of ion and protein concentration of Ps19, a shell protein from *Pteria sterna*, on calcium carbonate polymorph

Efecto de iones y concentración de proteína Ps19, una proteína de la concha de *Pteria sterna*, en los polimorfos de carbonato de calcio

Raquel Gabriela Arroyo-Loranca[1], Crisalejandra Rivera-Perez[2], Luis Hernandez-Adame[2], Ariel Arturo Cruz Villacorta[1], Jose Luis Rodriguez-Lopez[3], Norma Yolanda Hernandez-Saavedra[1]*

[1] Molecular Genetics Laboratory, Center for Biological Research of the Northwest (CIBNOR), La Paz, Baja California South, Mexico.
[2] CONACYT. Biological Research Center of the Northwest (CIBNOR), La Paz, Baja California Sur, Mexico.
[3] Advanced Materials Department, Potosi Institute for Scientific and Technological Research, San Luis Potosi, Mexico.

ABSTRACT

Calcium carbonate is present in many biological structures such as bivalve shells, which is composed mainly of two $CaCO_3$ polymorphs: calcite and aragonite. However, other forms of calcium carbonate exist like vaterite and amorphous calcium carbonate (ACC) that are not commonly reported. Polymorph selection is influenced by salt concentration, co-factor ions, and the presence of shell matrix proteins (SMPs) which regulates calcium carbonate deposition, among other factors. In this study, *in vitro* calcium carbonate crystallization of four different saline solutions (1: 40 mM $CaCl_2$, $MgCl_2$, 100 mM $NaHCO_3$; 2: $CaCl_2$, 100 mM Na_2CO_3; 3: 40 mM $CaCl_2$, $MgSO_4$, 100 mM Na_2CO_3; 4: $CaCl_2$/$MgCl_2$, 100 mM $NaHCO_3$) at two molarities (40 o 100 mM) was evaluated with increased concentrations of the Ps19 protein (0.2, 0.7 y 1.2 µg/µL), an insoluble extracted protein from the *Pteria sterna* shell, previously described as a promotor of aragonite platelet crystallization. *In vitro* crystallizations showed that Ps19 is capable to induce aragonite and calcite deposition in a dose-dependent manner, but also vaterite under certain conditions, acting as a promoter and inhibitor of crystallization. The results contribute to understand how Ps19 control precipitation of calcium polymorphs in the growth of the prismatic and nacre layer of the shell of *P. sterna*.

Keywords: Mollusk, shell protein, calcium carbonate, crystallization, nacre.

RESUMEN

El carbonato de calcio está presente en muchas estructuras biológicas, como la concha de bivalvo, que se compone principalmente de dos polimorfos de $CaCO_3$: calcita y aragonito. Sin embargo, existen otras formas de carbonato de calcio como vaterita y carbonato de calcio amorfo (ACC) que no se reportan comúnmente. La selección de polimorfos está influenciada por la concentración de sal, los iones cofactores y la presencia de proteínas de la matriz de la cubierta (SMP) que regulan la deposición de carbonato de calcio, entre otros factores. En este estudio, se evaluó la cristalización *in vitro* de carbonato de calcio de cuatro soluciones salinas diferentes (1: 40 mM $CaCl_2$, $MgCl_2$, 100 mM $NaHCO_3$; 2: $CaCl_2$, 100 mM Na_2CO_3; 3: 40 mM $CaCl_2$, $MgSO_4$, 100 mM Na_2CO_3; 4: $CaCl_2$/$MgCl_2$, 100 mM $NaHCO_3$) en dos molaridades (40 o 100 mM) con diferentes concentraciones la proteína Ps19 (0.2, 0.7 y 1.2 µg/µL) una proteína insoluble extraída de la concha de *Pteria sterna*, descrita anteriormente como promotora de la cristalización de plaquetas de aragonita. Las cristalizaciones *in vitro* mostraron que Ps19 es capaz de inducir la deposición de aragonita y calcita de forma dependiente de la dosis, pero también de vaterita en determinadas condiciones, actuando como promotor e inhibidor de la cristalización. Los resultados contribuyen a comprender cómo Ps19 controla la precipitación de polimorfos de calcio en el crecimiento de la capa prismática y de nácar de la concha de *P. sterna*.

Palabras clave: Molusco, proteína de la concha, carbonato, cristalización, nácar.

INTRODUCTION

In nature, three different anhydrous crystalline polymorphs of calcium carbonate ($CaCO_3$) exist (calcite, aragonite, and vaterite), two well-defined hydrous crystalline polymorphs (calcium carbonate monohydrate and calcium carbonate hexahydrate), and one amorphous form (ACC) (Meldrum and Colfen, 2008). The biological process by which $CaCO_3$ polymorphs are synthesized is called biomineralization (Kocot *et al.*, 2016; Song *et al.*, 2019). The shell of mollusks is the most studied $CaCO_3$ biomineral, because is the most abundant biomineral in nature and it is relatively easy to obtain (Demichelis *et al.*, 2018). The shell of bivalves is mainly composed of $CaCO_3$ (95 - 99 %) and an organic matrix containing acidic proteins, β-chitin, glycoproteins among other molecules (1 - 5 %) that function as a scaffold for mineral nucleation and plate formation (Wolf *et al.*, 2013).

The periostracum, the outer layer of the shell, is the first defense of the organism against external agents, it is not calcified and it is made of organic compounds (Kocot *et al.*, 2016). After the periostracum, the prismatic layer is composed mainly of calcite, the most stable and the second most abundant $CaCO_3$ polymorph in mollusks; it crystallizes in a

DOI:10.18633/biotecnia.v25i2.1885
*Author for correspondence: Norma Yolanda Hernandez Saavedra
e-mail: nhernan04@cibnor.mx
Received: October 31, 2022
Accepted: January 23, 2023

rhombohedral system making it a resistant and tough material to penetrate by forming prismatic structures (Bahn *et al.*, 2017). Beneath prismatic layer is the mother of pearl (nacre) layer, which is formed by aragonite. This polymorph has an orthorhombic form and it is less stable than calcite in isolated conditions, however, in the shell becomes a tougher, stiffer, and stronger material by assembling aragonite plates into structures that resemble a "brick-wall" (Evans, 2019). Besides calcite and aragonite, mollusks are capable to manipulate vaterite, the most unstable $CaCO_3$ polymorph present in the shell when their shell suffers a deformation (Wilt, 2005).

Vesicles of the mantle in mollusks act as ion storage sites of vaterite or amorphous calcium carbonate (ACC) (Addadi *et al.*, 2006). ACC is the hydrated form of $CaCO_3$ with a poorly order that contains magnesium (Addadi *et al.*, 2003), and acts a transient precursor of more stable $CaCO_3$ polymorphs (Politi *et al.*, 2008). There are two models that try to explain $CaCO_3$ nucleation. The first model, initiates with prenucleation, in which the ionic solution creates metastable clusters to begin the nucleation phase were single ions attach to the cluster and finally, depending on thermodynamic factors, calcite, vaterite, aragonite or ACC will be formed in the postnucleation phase. In second model, the prenucleation phase is pH-dependent to form a stable cluster, where the nucleation phase will begin depending on cluster concentration, its aggregation, or ion attachment. During the postnucleation phase, ACC is formed, and then calcite, aragonite, and vaterite are crystallized (Demichelis *et al.*, 2018).

Shell growth in mollusk is mediated by the shell matrix proteins (SMPs) from the mollusk shells. SMPs are synthesized in the mantle cells and released to the extrapallial fluid (EPF), between the mantle and the inner face of the shell (Wilt, 2005). The EPF contains a variety of ions which interact with SMPs (Wilt, 2005). SMPs are classified as soluble and insoluble proteins according to their solubility after the decalcification procedure used to extract them from the shell. Soluble proteins are rich in acidic hydrophilic residues, they are found between the crystals forming part of the scaffolding where $CaCO_3$ deposits (Levi-Kalisman *et al.*, 2001), while insoluble proteins are found inside the crystals, they have a high proportion of aliphatic amino acids forming short repetitive domains that have been associated with nucleation by promoting the interaction with acidic polyanionic soluble proteins (Wolf *et al.*, 2013; Du *et al.*, 2018).

Crystal polymorph growth in the mollusk shell is modulated by SMPs protein concentration and by the presence of cofactors. Low protein concentration (1 µg/mL) of some SMPs (e.g. PfN44), have been related to calcite growth with few aragonite crystals formation, but the increase in protein concentrations (2.5 µg/mL) have shown a total inhibition of aragonite deposition (Pan *et al.*, 2014). However, other SMPs such as Pif97 and pearlin showed inhibition of calcite crystal growth and ACC stabilization *in vitro* in increasing amounts of proteins (Montagnani *et al.*, 2011; Bahn *et al.*, 2015). This significant discrepancy between proteins could be related to their function in shell formation, either as a modulator of calcite or aragonite, or both. Besides protein concentration, Mg^{2+} ions have been reported to modulate aragonite growth (Pan *et al.*, 2014; Ma and Feng, 2015). Low magnesium content induces calcite growth while high magnesium content induces the formation of aragonite (Raz *et al.*, 2000). In *Hyriopsis cumingii*, the water-soluble matrix of aragonite pearls formed little needle-like crystals, accompanied by irregular Mg-calcite structures when low magnesium is present (10 mM). However, in the presence of high magnesium ions (40 mM), quasi-spherical aragonite aggregates appear from needle-like crystals, coexisting with a few Mg-calcites (Ma and Feng, 2015).

Other proteins, such as SPARC (secreted protein acidic and rich in cysteine), from *P. fucata*, participate in nacre formation by stabilizing vaterite to inhibit calcite, as well as by forming aragonite in presence of Mg^{2+} or other proteins (Xie *et al.*, 2016). Nevertheless, there are also proteins able to produce aragonite crystals in presence of magnesium or calcium (40 mM) as cofactors, such as the glycoprotein Ps19 from *Pteria sterna* (Arroyo-Loranca *et al.*, 2020). Even when this information suggests that SMPs can to modulate crystal polymorphs by protein and ion concentrations, further research is needed to support this statement since the crystallization assay previously reported in several SMPs are not always comparable due to the different preparations used.

To understand the biomineralization processes is necessary to known the mechanism used by SMPs to control crystal deposition, either by protein and/or ion concentration. Therefore, this research aimed to understand the role of Ps19, a novel SMPs, with no homology to previously described proteins, on crystal deposition, by evaluating the effect of protein concentration (0.2 – 1.2 $\mu g \cdot \mu L^{-1}$) and cofactor concentration (40/100 mM of $MgCl_2$, $CaCl_2$, 1:1 $MgCl_2$:$CaCl_2$ and $MgSO_4$) on crystal polymorph deposition *in vitro*. The results indicate Ps19 is an effective promoter of aragonite and calcite in the presence of $MgCl_2$ and $CaCl_2$, respectively. Also, this positive modulation is dependent on protein and ion concentration. Thus, this suggests that Ps19 may be involved in the prismatic and nacre layer of *Pteria sterna*.

MATERIAL AND METHODS

Ps19 extraction from *P. sterna* shell

Perlas del Cortez S. de R.L. MI., granted three adult organisms from Bahia de La Paz, B.C.S. Oysters were transported to the Centro de Investigaciones Biológicas del Noroeste S.C. facilities where shells were pulverized, and 20 g of the powder were decalcified with cold acetic acid (10 % *v/v*) at 4 °C and constant stirring according to Montagnani *et al*. (2011); later, the solution was centrifuged to obtain the Acetic Soluble Matrix (ASM) and the Acetic Insoluble Matrix (AIM) as described by Arroyo-Loranca *et al*. (2020).

SDS-PAGE

The AIM, and later the Ps19 protein were loaded into a sodium dodecyl sulphate polyacrylamide gel electrophoresis (SDS-PAGE) according to Laemmli (1970), the samples were trea-

ted as previously described by Arroyo-Loranca *et al*. (2020). A quantity of 60.3 µg of AIM and 15.1 µg of *P. sterna* shell Ps19 per gel were loaded. An SDS-PAGE molecular weight marker was used for molecular weight comparison (Broad range, Bio-Rad 161-0317). Electrophoresis was conducted at 90-V at room temperature, using a Bio-Rad electrophoresis unit (Protean II). After electrophoresis, the gel was stained with Coomassie Brilliant Blue R250 (CBB) for 2 h, washed out, and analyzed using a Chemi Doc XRS (Bio-Rad).

Protein quantification by densitometry

Ps19 quantification was performed by pixel densitometry in a 16 % SDS-PAGE gel stained with CBB. A protein standard curve was constructed with ovalbumin protein (0.25 - 8.0 $\mu g \cdot \mu L^{-1}$) as described by Arroyo-Loranca *et al*. (2020). A Chemi Doc XRS (Bio-Rad, California, USA) was used to analyze the image of the gel to obtain the linear equation (1) and calculate the quantity of the proteins present in the samples.

$$y = 5.31 \times 10^{-6}x - 0.94 \quad (1)$$

The Ps19 protein was purified from the AIM of *P. sterna* shell by four preparative polyacrylamide gel electrophoresis according to the Mini-Prep Cell manual (Bio-Rad, 491 Prep Cell) according to Arroyo-Loranca *et al*. (2020). A total of 100 fractions of 200 µL each were collected, selected fractions were loaded into an SDS-PAGE polyacrylamide gel (16 %) to identify the fractions containing the Ps19 protein. Then, fractions containing Ps19 were pooled, concentrated, and cleaned from the electrophoresis buffer by centrifugation with an Amicon Ultra-4 filter (EMD Millipore) as described by Arroyo-Loranca *et al*. (2020). The purified protein (380 µL) was stored at -20 °C.

Ps19 identification

The purified Ps19 was analyzed to verify the properties of the previously characterized protein by Arroyo-Loranca *et al*. (2020). The molecular weight of Ps19 was calculated through its Rf, the calcium-binding capability was corroborated by the Stains-All stain (Green *et al*., 1973) after electrophoresis separation as previously described. A total of 15.1 µg of Ps19 in an SDS-PAGE 16 % polyacrylamide gel was used.

Calcium carbonate crystallization *in vitro*

Calcium carbonate ($CaCO_3$) crystallization in the presence of Ps19 was evaluated by the incubation of four saturated solutions and three differente protein concentrations that shown in Table 1. Each combination (10 µL of Ps19 and 50 µL of saturated solution) was placed over a glass coverslip inside a Petri dish with absorbent paper at the bottom to prevent condensation. The Petri dishes were sealed with parafilm, placed into a container, and incubated for 30 days at 4 °C. Controls and solutions 1 to 4 (50 µL) were mixed with sterile distilled water (10 µL) instead of Ps19 and the protein by itself (10 µL) was mixed with 50 µL of sterile distilled water. The morphology of the crystals was analyzed by Scanning Electron Microscopy (SEM) at the Electronic Microscopy Laboratory at Centro de Investigaciones Biológicas del Noroeste (CIBNOR), México. Every experiment and analysis were performed by triplicate.

Raman spectroscopy

Raman spectra were identified by using an InVia micro-Raman spectrometer (Renishaw, Gloucestershire, UK) with an excitation line of 532 nm provided by a YAG laser of 100 mW and a spot size of 2 µm x 2 µm. For measurements, the slits were set at 200 µm and a 100× objective was used. The crystals were scanned by triplicate for 90 seconds from 100 to 1900 cm^{-1} for the specific identification.

RESULTS

Ps19 isolation and quantification

The acid-soluble (ASM) and acid-insoluble (AIM) matrixes were obtained by extraction with cold acetic acid. The AIM was separated by denaturalizing electrophoresis and visualized by CBB stain (Figure 1A). The Ps19 protein was identified

Table 1. Conditions for $CaCO_3$ crystallization *in vitro* in the presence of Ps19.
Tabla 1. Condiciones para la cristalización de $CaCO_3$ *in vitro* en presencia de Ps19.

Solution	**Salt**	**Cofactor**	Molarity of the cofactor (Mm)	pH	Ps19 ($\mu g \cdot \mu L^{-1}$)	Expected $CaCO_3$ polymorph	Reference
1	40 mM $CaCl_2$, 100 mM NaHCO3	$MgCl_2$	40 or 100	8.2	0.2 0.7 1.2	Aragonite	(Weiss *et al.*, 2000)
2	100 mM Na_2CO3	$CaCl_2$	40 or 100	8.2	0.2 0.7 1.2	Calcite	(Declet *et al.*, 2016)
3	40 mM $CaCl_2$, 100 mM Na_2CO3	$MgSO_4$	40 or 100	8.2	0.2 0.7 1.2	Aragonite	(Nielsen *et al.*, 2016)
4	100 mM NaHCO3	$CaCl_2$ and $MgCl_2$	40 or 100	8.2	0.2 0.7 1.2	Calcite/ aragonite	(Loste *et al.*, 2003)

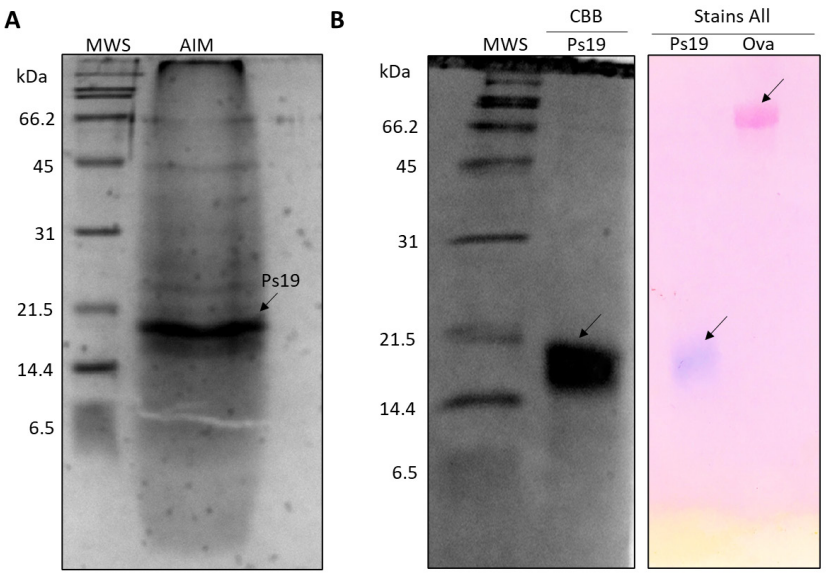

Figure 1. Acetic insoluble matrix (AIM) from the shell of ***Pteria sterna*.** (A) AIM in a SDS-PAGE 16 % polyacrylamide gel stained with CBB. MWS: molecular weight standard (Bio-Rad 1610317), AIM: acetic-acid insoluble matrix proteins, the arrow indicates the Ps19 protein. (B) Isolated Ps19 shell protein from *P. sterna* and Ca^{2+} binding capability (Stain all). Ova: ovalbumin (negative control).
Figura 1. Matriz acética insoluble (AIM) de la concha de *Pteria sterna*. (A) AIM en un gel de poliacrilamida SDS-PAGE al 16 % teñido con CBB. MWS: estándar de peso molecular (Bio-Rad 1610317), AIM: proteínas de matriz insolubles en ácido acético, la flecha indica la proteína Ps19. (B) Proteína de la concha Ps19 de P. sterna y capacidad de unión a calcio (tinción Stain all). Ova: Ovoalbúmina (control negativo).

by determining its molecular weight (~19 kDa) through its relative mobility along with the gel.

The Ps19 protein was purified by preparative electrophoresis (Figure 1B). From the four electrophoreses, a total of 576 µg of Ps19 were purified from 3.4 mg of unpurified protein present in the AIM extracted from the pulverized shell, having a protein (Ps19) with a 17 % yield and 94 % purity (Table 2).

The amount of purified Ps19 was determined by pixel densitometry (Figure 1B). The CBB and Stains-All stains corroborated that the isolated protein was Ps19, which had the expected molecular weight (19 kDa) and presented Ca^{2+} binding capability (Figure 1B) as described by Arroyo-Loranca *et al*. (2020).

$CaCO_3$ crystallization *in vitro*

The modulation of $CaCO_3$ crystal polymorph formation by Ps19 was evaluated by SEM. The Ps19 protein was able to produce calcite crystals when $MgCl_2$ was used as a cofactor at 40 and 100 mM (Figure 2). At 40 mM $MgCl_2$, Ps19 crystallized calcite crystal plates in their typical geometric shape with smooth sides (Figure 2 F-H), which were comparable in size than those observed in the controls (Figure 2E, 3I-K). At 100 mM $MgCl_2$ (Figure 2), only hexagonal vaterite was formed, plates were more structured, and stacked forming platelet interlocks (white arrow, Figure 2B). Increase of Ps19 concentration displayed crystal inhibition at 40 mM when protein was set at 1.2 $\mu g \cdot \mu L^{-1}$, however, this behavior was not observed at 100 mM $MgCl_2$ and $CaCO_3$ crystals presented diamond shape instead of hexagonal, as seen at 0.2 and 1.2 $\mu g \cdot \mu L^{-1}$ Ps19 concentration.

The addition of Ps19 to the solution containing 40 and 100 mM $CaCl_2$ did not generate crystals of calcite or aragonite (Figure 3). At 40 mM rod-like crystals were observed (Figure 3F, G), while high $CaCl_2$ concentration displayed scarce rod-like crystals (Figure 3B) and isolated polycrystalline deposits generating halos or inhibition zones (Figure 3C). The increase of Ps19 concentration at 40 and 100 mM did not produce any significant pattern on crystal deposition.

Saturated solution containing $MgSO_4$ as source of Mg^{2+} ion resulted in $CaCO_3$ precipitation as ACC (Figure 4). At 40 mM $MgSO_4$, ACC polymorph was predominant in the solution, however small aragonite structures were visible at 0.2

Table 2. Ps19 purification from *Pteria sterna* shell.
Tabla 2. Purificación de Ps19 a partir de la concha de *Pteria sterna*.

Species	Step	Total Protein (mg)	Ps19 (mg)	Yield (%)	Purity (%)
Pteria sterna	Crude extract	3.456	3.016	100	87
	Preparative electrophoresis	3.016	0.616	20	94
	Amicon-washed concentrate	0.576	0.576	19	94

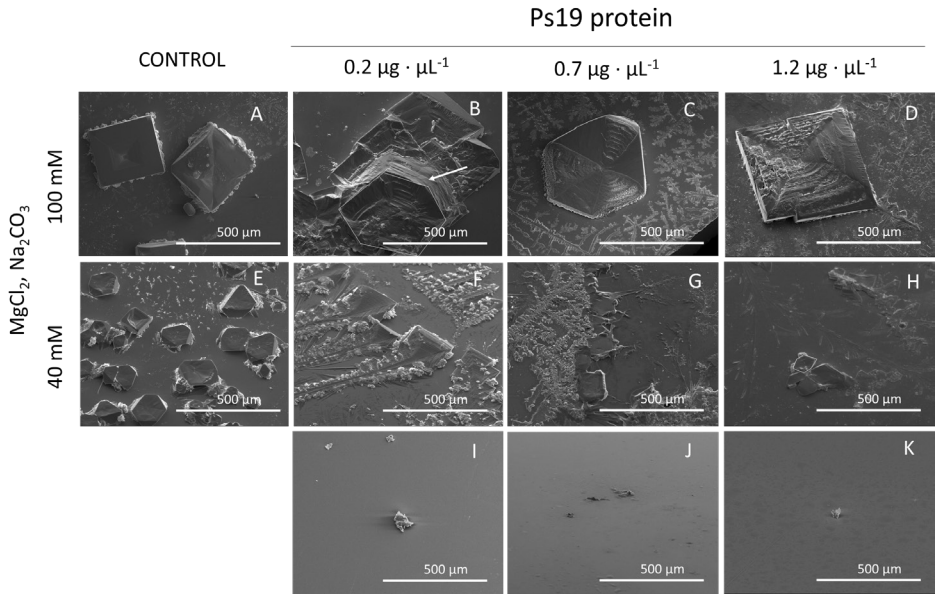

Figure 2. SEM micrographs of calcium carbonate crystals growth *in vitro* in the presence of 40 mM $CaCl_2$, Mg^{2+} ion (40 and 100 mM), 100 mM $NaHCO_3$ and Ps19 at increasing concentrations (µg·µL^{-1}). First panel from left to right (A, E) Negative controls without Ps19; 100 mM Mg^{2+} ion in presence of (B) 0.2 µg·µL^{-1}, (C) 0.7 µg·µL^{-1}, (D) 1.2 µg·µL^{-1} Ps19; 40 mM Mg^{2+} ion in presence of (B) 0.2 µg·µL^{-1}, (C) 0.7 µg·µL^{-1}, (D) 1.2 µg·µL^{-1} Ps19; (I-K) protein alone without salt. Scale bars are 500 µm. Hexagonal structures are shown in white lines, and arrow indicates platelet interlocks. Each picture is representative of three independent crystallization assays.

Figura 2. Micrografías SEM del crecimiento de cristales de carbonato de calcio in vitro en presencia de $CaCl_2$ 40 mM, iones Mg^{2+} (40 y 100 mM), $NaHCO_3$ 100 mM y Ps19 a concentraciones crecientes (µg·µL^{-1}). Primer panel de izquierda a derecha (A, E) Controles negativos sin Ps19; ion Mg^{2+} 100 mM en presencia de (B) 0,2 µg·µL^{-1}, (C) 0,7 µg·µL^{-1}, (D) 1,2 µg·µL^{-1} Ps19; ion Mg^{2+} 40 mM en presencia de (B) 0,2 µg·µL^{-1}, (C) 0,7 µg·µL^{-1}, (D) 1,2 µg·µL^{-1} Ps19; (I-K) proteína sola sin sal. Las barras de escala son de 500 µm. Las estructuras hexagonales se muestran en líneas blancas y la flecha indica interbloqueos de plaquetas. Cada imagen es representativa de tres ensayos de cristalización independientes.

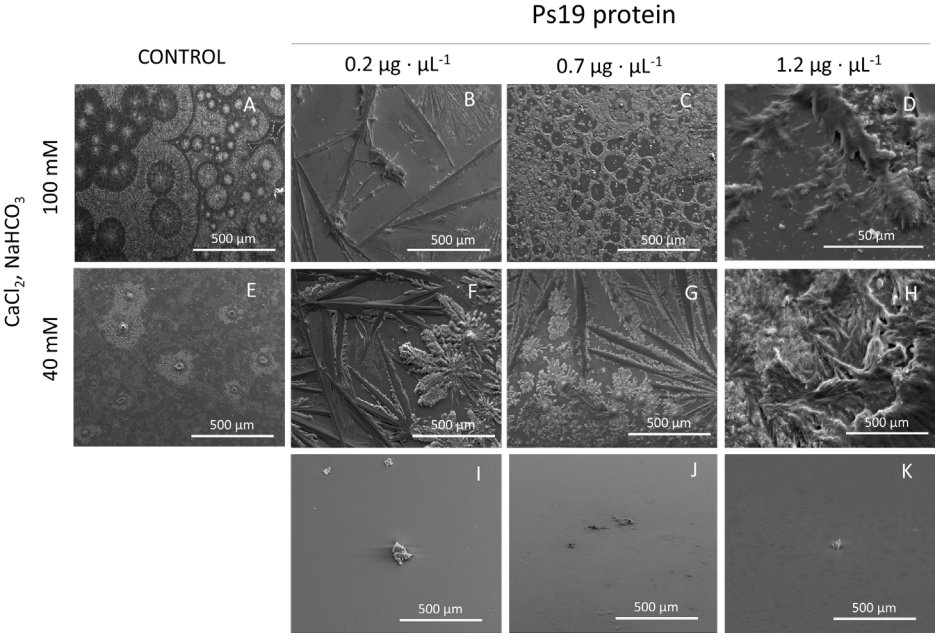

Figure 3. SEM micrographs of calcium carbonate crystals growth *in vitro* in the presence of Ca^{2+} ion (40 and 100 mM), 100 mM Na_2CO_3 and Ps19 at increasing concentrations (µg·µL^{-1}). First panel from left to right (A, E) Negative controls without Ps19; 100 mM Ca^{2+} ion in presence of Ps19 protein (B) 0.2 µg·µL^{-1}, (C) 0.7 µg·µL^{-1}, (D) 1.2 µg·µL^{-1} Ps19; 40 mM Ca^{2+} ion in presence of (B) 0.2 µg·µL^{-1}, (C) 0.7 µg·µL^{-1}, (D) 1.2 µg·µL^{-1} Ps19; (I-K) protein alone without salt. Scale bars are 500 µm. Each picture is representative of three independent crystallization assays.

Figura 3. Micrografías SEM del crecimiento in vitro de cristales de carbonato de calcio en presencia de ion Ca^{2+} (40 y 100 mM), Na_2CO_3 100 mM y Ps19 a concentraciones crecientes (µg·µL^{-1}). Primer panel de izquierda a derecha (A, E) Controles negativos sin Ps19; ion Ca^{2+} 100 mM en presencia de (B) 0,2 µg·µL^{-1}, (C) 0,7 µg·µL^{-1}, (D) 1,2 µg·µL^{-1} Ps19; ion Ca^{2+} 40 mM en presencia de (B) 0,2 µg·µL^{-1}, (C) 0,7 µg·µL^{-1}, (D) 1,2 µg·µL^{-1} Ps19; (I-K) proteína sola sin sal. Las barras de escala son de 500 µm. Cada imagen es representativa de tres ensayos de cristalización independientes.

and 0.7 μg·μL^{-1} Ps19 protein (Figure 4F-H). But, at 100 mM $MgSO_4$ no rhombohedral or even facetted crystals at all were spotted, instead agglomerations of spheres were observed at all Ps19 concentrations tested (Figure 4B-D).

Finally, when $CaCl_2$/$MgCl_2$ (1:1 ratio) were present in the crystallization assay formed scarce crystal structures and a thin film was present over all crystal preparations (Figure 5). At 40 mM $CaCl_2$/$MgCl_2$, an aragonite tablet was observed at 0.7 μg·μL^{-1} (Figure 5G), while at 100 mM $CaCl_2$/$MgCl_2$, only aragonite crystals were observed at 0.7 μg·μL^{-1} and 1.2 μg·μL^{-1} (Figure 5C,D), which were 100 μm size.

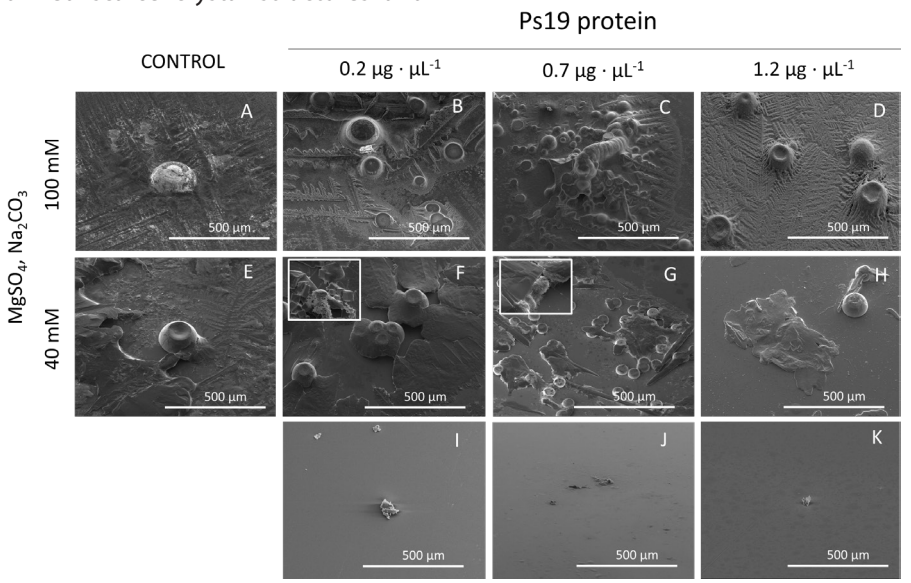

Figure 4. SEM micrographs of calcium carbonate crystals growth *in vitro* in the presence of 40 mM $CaCl_2$, Mg^{2+} ion (40 and 100 mM) as $MgSO_4$, 100 mM Na_2CO_3 and Ps19 at increasing concentrations (μg·μL^{-1}). First panel from left to right (A, E) Negative controls without Ps19; 100 mM Mg^{2+} ion in presence of (B) 0.2 μg·μL^{-1}, (C) 0.7 μg·μL^{-1}, (D) 1.2 μg·μL^{-1} Ps19; 40 mM Mg^{2+} ion in presence of (B) 0.2 μg·μL^{-1}, (C) 0.7 μg·μL^{-1}, (D) 1.2 μg·μL^{-1} Ps19; (I-K) protein alone without salt. Scale bars are 500 μm, inlets are 50 μm size. Each picture is representative of three independent crystallization assays.

Figura 4. Micrografías SEM del crecimiento de cristales de carbonato de calcio in vitro en presencia de $CaCl_2$ 40 mM, iones Mg^{2+} (40 y 100 mM) como $MgSO_4$, Na_2CO_3 100 mM y Ps19 a concentraciones crecientes (μg·μL^{-1}). Primer panel de izquierda a derecha (A, E) Controles negativos sin Ps19; ion Mg^{2+} 100 mM en presencia de (B) 0.2 μg·μL^{-1}, (C) 0.7 μg·μL^{-1}, (D) 1.2 μg·μL^{-1} Ps19; ion Mg^{2+} 40 mM en presencia de (B) 0.2 μg·μL^{-1}, (C) 0.7 μg·μL^{-1}, (D) 1.2 μg·μL^{-1} Ps19; (I-K) proteína sola sin sal. Las barras de escala son de 500 μm, las entradas tienen un tamaño de 50 μm. Cada imagen es representativa de tres ensayos de cristalización independientes.

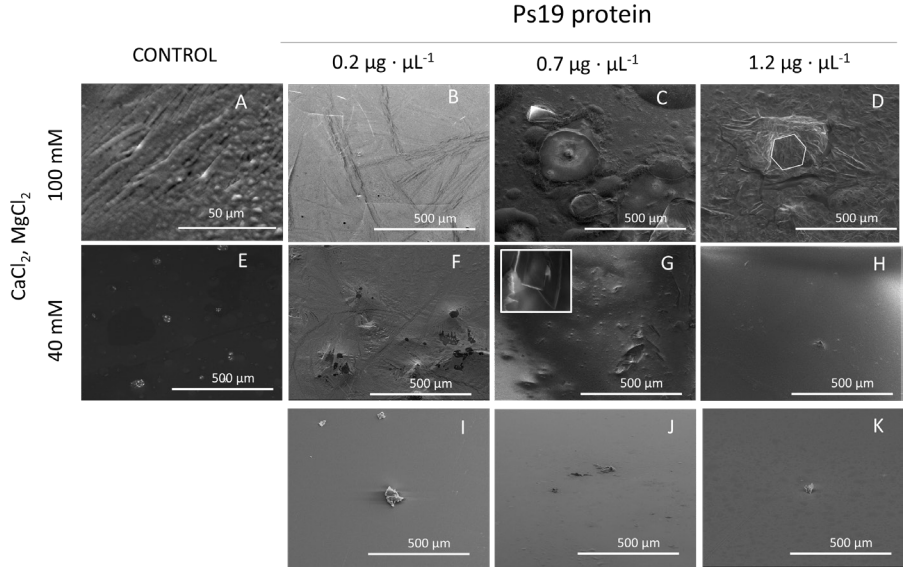

Figure 5. SEM micrographs of calcium carbonate crystals growth *in vitro* in the presence of $CaCl_2$ and $MgCl_2$ (40 and 100 mM), 100 mM $NaHCO_3$ and Ps19 at increasing concentrations (μg·μL^{-1}). First panel from left to right (A, E) Negative controls without Ps19; 100 mM $CaCl_2$/$MgCl_2$ in presence of (B) 0.2 μg·μL^{-1}, (C) 0.7 μg·μL^{-1}, (D) 1.2 μg·μL^{-1} Ps19; 40 mM $CaCl_2$/$MgCl_2$ in presence of (B) 0.2 μg·μL^{-1}, (C) 0.7 μg·μL^{-1}, (D) 1.2 μg·μL^{-1} Ps19; (I-K) protein alone without salt. Scale bars are 500 μm, inlets are 50 μm size. Each picture is representative of three independent crystallization assays.

Figura 5. Micrografías SEM del crecimiento *in vitro* de cristales de carbonato de calcio en presencia de $CaCl_2$ y $MgCl_2$ (40 y 100 mM), $NaHCO_3$ 100 mM y Ps19 a concentraciones crecientes (μg·μL^{-1}). Primer panel de izquierda a derecha (A, E) Controles negativos sin Ps19; $CaCl_2$/$MgCl_2$ 100 mM en presencia de (B) 0.2 μg·μL^{-1}, (C) 0.7 μg·μL^{-1}, (D) 1.2 μg·μL^{-1} Ps19; $CaCl_2$/$MgCl_2$ 40 mM en presencia de (B) 0.2 μg·μL^{-1}, (C) 0.7 μg·μL^{-1}, (D) 1.2 μg·μL^{-1} Ps19; (I-K) proteína sola sin sal. Las barras de escala son de 500 μm, las entradas tienen un tamaño de 50 μm. Cada imagen es representativa de tres ensayos de cristalización independientes.

Raman analysis

Raman measurements confirmed the presence of $CaCO_3$ polymorphs (Figure 6). The spectra show characteristics peaks belonging to the internal vibration mode of co_3^{2-} (at around 1080 cm^{-1}) and the related between Ca^{2+} with co_3^{2-} (Han *et al.*, 2017). The signal differences from 100 to 400 cm^{-1} derived from the different vibration modes of Ca^{2+} and co_3^{2-} in calcite and aragonite. In aragonite, the interatomic distances between Ca^{2+} and co_3^{2-} are smaller than that of calcite; hence, the bonds between Ca^{2+} and co_3^{2-} are stronger and the Raman signals appear at lower-frequency vibrational mode than that of calcite (Arroyo-Loranca *et al.*, 2020). Moreover, is interesting to observe the presence of a triplet formed in the region from 1070 to 1090 cm^{-1}. These vibrations are characteristic of the vaterite formation that was confirmed by the additional vibrations modes from 700 to 790 cm^{-1} belonging to the internal translational modes of in-plane bending of the carbonate ions in vaterite (Soldati *et al.*, 2008). In this sense, Figure 6 shows the Raman spectra of $CaCO_3$ polymorphs when $MgCl_2$ was used as a cofactor at 40 and 100 mM. At 40 mM, the control (solution without protein) shows a triplet from 1070 to 1090 cm^{-1} assigned to the vaterite formation, while a protein concentration of 0.2 and 0.7 $\mu g \cdot \mu L^{-1}$ show vibration modes in the range of 700 and 200 cm^{-1} assigned to the calcite formation.

The Raman spectra of samples using $CaCl_2$ as a cofactor are shown in Figure 7. Here we observe a single vibration mode in the region from 1060 to 1080 cm^{-1}corresponding to co_3^{2-} which indicates only a co_3^{2-}deposition without any structured crystals formation as can be observed by SEM (Figure 3). Figure 8 shows the Raman spectra of samples using $MgSO_4$ as a cofactor. The spectra show vibration modes in the region from 900 to 1070 cm^{-1} and from 230 to 640 cm^{-1}. These vibrations modes can be assigned to ACC polymorphs. Finally, the use of $CaCl_2$ and $MgCl_2$ as a cofactor, do not show any crystal formation.

DISCUSSION

The shell growth in Mollusk has been described to start with the precipitation of ACC, which is known to surround aragonite platelets in gastropods (e.g. *Haliotis laevigata*) and bivalves (e.g. *Pinctada margaritifera* and *Atrina rigida*) indica-

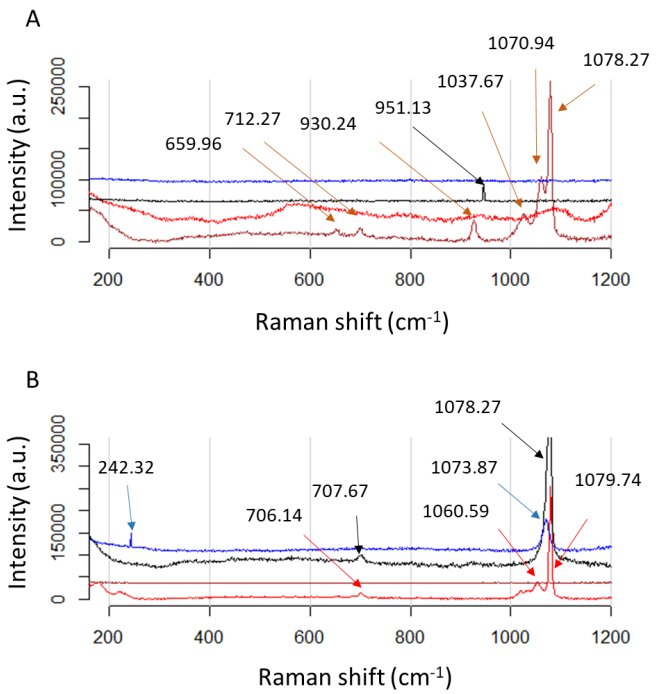

Figure 6. Raman spectra of calcite and vaterite formation by using Ps19 protein and $MgCl_2$ as a cofactor. Calcium carbonate crystals growth *in vitro* in the presence of $MgCl_2$ Na_2CO3. (A) 100 mM and (B) 40 mM, respectively. Color line indicate salts preparations, red line: salt without protein added, black: salt in the presente of 0.2 $\mu g \cdot \mu L^{-1}$, blue: salt in the presence of 0.7 $\mu g \cdot \mu L^{-1}$, brown: salt in the presence of 1.2 $\mu g \cdot \mu L^{-1}$. Color arrows indicate the peaks for each salt preparation.

Figura 6. Espectros Raman de formación de calcita y vaterita usando proteína Ps19 y $MgCl_2$ como cofactor. Crecimiento de cristales de carbonato de calcio *in vitro* en presencia de $MgCl_2$ Na_2CO3. (A) 100 mM y (B) 40 mM, respectivamente. La línea de color indica preparaciones de sales, línea roja: sal sin proteína añadida, negra: sal en presencia de 0.2 $\mu g \cdot \mu L^{-1}$, azul: sal en presencia de 0.7 $\mu g \cdot \mu L^{-1}$, marrón: sal en presencia de 1.2 $\mu g \cdot \mu L^{-1}$. Las flechas de color indican los picos para cada preparación de sal.

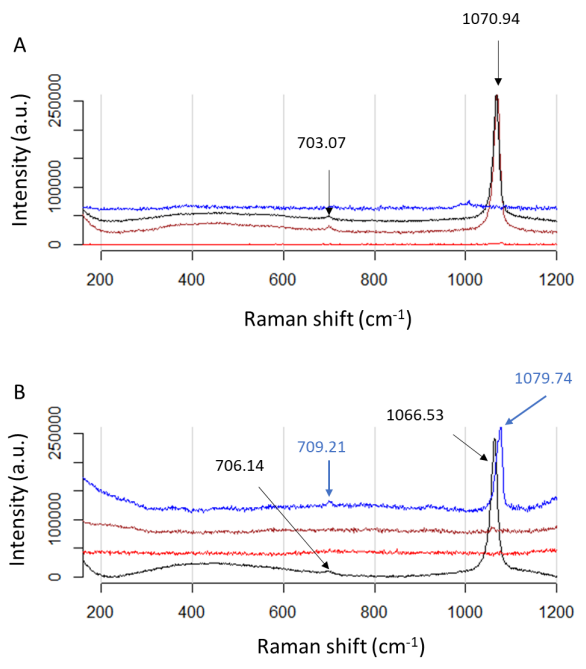

Figure 7. Raman spectra of carbonates deposition by using Ps19 protein and $CaCl_2$ as a cofactor. Calcium carbonate crystals growth *in vitro* in the presente of $CaCl_2$ $NaHCO_3$ (A) 100 mM and (B) 40 mM, respectively. Color line indicate salts preparations, red line: salt without protein added, black: salt in the presente of 0.2 $\mu g \cdot \mu L^{-1}$, blue: salt in the presence of 0.7 $\mu g \cdot \mu L^{-1}$, brown: salt in the presence of 1.2 $\mu g \cdot \mu L^{-1}$. Color arrows indicate the peaks for each salt preparation.

Figura 7. Espectros Raman de deposición de carbonatos usando proteína Ps19 y $CaCl_2$ como cofactor. Crecimiento de cristales de carbonato de calcio in vitro en presencia de $CaCl_2$ $NaHCO_3$ (A) 100 mM y (B) 40 mM, respectivamente. La línea de color indica preparaciones de sales, línea roja: sal sin proteína añadida, negra: sal en presencia de 0.2 $\mu g \cdot \mu L^{-1}$, azul: sal en presencia de 0.7 $\mu g \cdot \mu L^{-1}$, marrón: sal en presencia de 1.2 $\mu g \cdot \mu L^{-1}$. Las flechas de color indican los picos para cada preparación de sal.

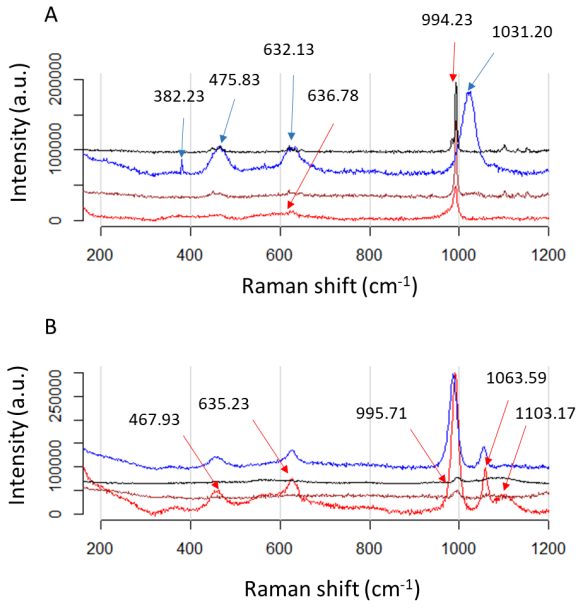

Figure 8. Raman spectra of ACC polymorphs by using Ps19 protein and $MgSO_4$ as a cofactor. Calcium carbonate crystals growth *in vitro* in the presence of A) 100 mM $MgSO_4$ Na_2CO_3 or B) 40 mM $MgSO_4$ Na_2CO_3. Color line indicate salts preparations, red line: salt without protein added, black: salt in the presente of 0.2 µg·µL^{-1}, blue: salt in the presence of 0.7 µg·µL^{-1}, brown: salt in the presence of 1.2 µg·µL^{-1}. Color arrows indicate the peaks for each salt preparation.

Figura 8. Espectros Raman de polimorfos de ACC usando proteína Ps19 y $MgSO_4$ como cofactor. Crecimiento de cristales de carbonato de calcio *in vitro* en presencia de A) 100 mM de $MgSO_4$ Na_2CO_3, B) 40 mM de $MgSO_4$ Na_2CO_3 La línea de color indica preparaciones de sales, línea roja: sal sin proteína añadida, negra: sal en presencia de 0.2 µg·µL^{-1}, azul: sal en presencia de 0.7 µg·µL^{-1}, marrón: sal en presencia de 1.2 µg·µL^{-1}. Las flechas de color indican los picos para cada preparación de sal.

ting a nascent growing platelet (Nassif *et al.*, 2005; Rousseau *et al.*, 2009). ACC is a highly metastable phase, which is often found hydrated, and after dehydration, transforms to calcite, aragonite, or vaterite (Radha *et al.*, 2010). Divalent ions have been found to affect the crystallization rates and pathways of ACC (Tobler *et al.*, 2015). In Mollusk shells, Mg^{2+} ion is 2.55 % of their weight (Huang *et al.*, 2018). This ion is known to stabilize ACC forming a complex (Mg-ACC) and reducing their reactivity to form polymorphs or calcite or aragonite, however, aragonite can be detectable since Mg^{2+} is known to suppress calcite growth (Davis *et al.*, 2000). In our study, the mixture of the Ps19 with the saturated solution containing 40 and 100 mM $MgSO_4$, respectively (Figure 4), resulted in the formation of imperfect spherical morphologies, which has been previously described (Xu *et al.*, 2014). However, this was not observed when $MgCl_2$ was used as a cofactor (Figure 2). This may be explained by the hydration capability of $MgSO_4$ (heptahydrate) compared to $MgCl_2$ (hexahydrated), acting as an inhibitor of calcite by occlusion of Mg inside the platelet, leading a less hydratated form of $CaCO_3$ (Nielsen *et al.*, 2016).

The transition of ACC to calcite and aragonite in Mollusk is modulated by Mg^{2+} ions and SMPs (Ma and Feng, 2015). In our study, Ps19 was able to induce well-formed aragonite platelets, being the bigger aragonite crystal those found at 100 mM $MgCl_2$ (Figure 2). However, the inhibition observed at 40 mM $MgCl_2$, and the less structured aragonite crystal at 100 mM $MgCl_2$ when 1.2 µg·µL^{-1} Ps19 was used (Figure 2D, H), suggest that Ps19 can act as an inhibitor of crystal growth besides its role as a crystallization inductor, this dual role may be ion and protein concentration-dependent as has been suggested previously (Arroyo-Loranca *et al.*, 2020). Similar results have been observed in Prismalin-14, Pif97, KRMP-3, and rPNU9 from *P. fucata* (Suzuki *et al.*, 2004; Bahn *et al.*, 2015; Liang *et al.*, 2016; Kong *et al.*, 2019).

SMPs related to prismatic layer growth of the shell have been found to form strictly calcite crystal at low $CaCl_2$ concentration and to be able to inhibit aragonite platelet growth, e.g. Prisilkin-39 from *P. fucata* (Kong *et al.*, 2009). However, Ps19 have been proved previously to produce calcite (Arroyo-Loranca *et al.*, 2020) at low $CaCl_2$. Interestingly, putative inhibition zones of crystal growth were observed in this study at high $CaCl_2$ concentration and 0.7 µg·µL^{-1} of Ps19 (Figure 3C), a behavior also been observed in other SMPs such as rPif97 from *P. fucata* (Bahn *et al.*, 2015), suggesting that calcite crystal deposition may be protein dose-dependent. The capability of Ps19 to produce calcite and aragonite using different ions suggest that Ps19 is associated to the formation of the prismatic and nacre layer in *P. sterna*, as has been described in other SMPs such as Lys-rich matrix protein family from *P. fucata* (Liang *et al.*, 2016) and nacrein from the Pacific oyster *Crassostrea gigas* (Song *et al.*, 2014).

Besides modulation by a single ion, the growth of calcite and aragonite is dependent on the Mg^{2+} and Ca^{2+} molar ratio (Loste *et al.*, 2003). An increase in the Mg^{2+} molar ratio leads to the growth of a hydrated phase of $CaCO_3$ at the surface of the solution, while at the base of the crystallization assay produces calcite and aragonite from 2:1, 3:1 and 4:1 of Mg:Ca (Loste *et al.*, 2003). For Ps19, a molar ratio of 1:1 leads to the production of a thin film and scarce crystal growth with undefined structures at both concentration, 40 and 100 mM, however calcitic and aragonite structures were visible at 0.7 and 1.2 µg·µL^{-1} of Ps19, these results lead to the hypothesis that Ps19 may react with the salts and inhibit the crystal growth of either calcite or aragonite, and the crystals formed are the result of dehydrated spots in the crystallization assay, however further experiments are required corroborate this hypothesis.

CONCLUSIONS

In contrast to other SMPs described in Mollusk, which promote one kind of calcium carbonate polymorph (e.g. aragonite or calcite), Ps19 is a novel protein capable to induce calcite and aragonite crystals in a dose-dependent manner at different ion concentrations, acting as a promoter of aragonite in presence of $MgCl_2$ and as a promoter of calcite in presence of $CaCl_2$, suggesting that Ps19 may play an important role in the prismatic and nacre layer of the shell of *P. sterna*.

ACKNOWLEDGMENTS

The authors are grateful to Delia Irene Rojas Posadas for her technical assistance, as well as to M.C. Beatríz Adriana Rivera Escoto for the measurements with the Raman spectrometer from the National Laboratory for Nanoscience and Nanotechnology Research (LINAN) at IPICYT, A.C.; also to CONACyT for the fellowship grant number 358437.

REFERENCES

Addadi, L., Joester, D., Nudelman, F. and Weiner, S. 2006. Mollusk shell formation: A source of new concepts for understanding biomineralization processes. Chemistry. 12: 980-987.

Addadi, L., Raz, S. and Weiner, S. 2003. Taking advantage of disorder:Amorphus calcium carbonate and its roles in biomineralization. Advanced Materials. 15: 959-970.

Arroyo-Loranca, R. G., Hernandez-Saavedra, N. Y., Hernandez-Adame, L. and Rivera-Perez, C. 2020. Ps19, a novel chitin binding protein from *Pteria sterna* capable to mineralize aragonite plates *in vitro*. PLoS One. 15: 1-15.

Bahn, S. Y., Jo, B. H., Choi, Y. S. and Cha, H. J. 2017. Control of nacre biomineralization by pif80 in pearl oyster. Science Advances. 3: e1700765.

Bahn, S. Y., Jo, B. H., Hwang, B. H., Choi, Y. S. and Cha, H. J. 2015. Role of pif97 in nacre biomineralization: *In vitro* characterization of recombinant pif97 as a framework protein for the association of organic–inorganic layers in nacre. Crystal Growth & Design. 15: 3666-3673.

Davis, K. J., Dove, P. M. and De Yoreo, J. J. 2000. The role of Mg^{2+} as an impurity in calcite growth. Science. 290: 1134-1137.

Declet, A., Reyes, E. and Suárez, O. M. 2016. Calcium carbonate precipitation : A review of the carbonate crystallization process and applications in bioinspired composites. Reviews on Advanced Materials Science. 44: 87-107.

Demichelis, R., Schuitemaker, A., Garcia, N. A., Koziara, K. B., De La Pierre, M., Raiteri, P. and Gale, J. D. 2018. Simulation of crystallization of biominerals. Annual Review of Materials Research. 48: 327-352.

Du, J., Liu, C., Xu, G., Xie, J., Xie, L. and Zhang, R. 2018. Fam20c participates in the shell formation in the pearl oyster, *Pinctada fucata*. Scientific Reports. 8: 3563.

Evans, J. S. 2019. Composite materials design: Biomineralization proteins and the guided assembly and organization of biomineral nanoparticles. Materials. 12: 581-591.

Green, M. R., Pastewka, J. V. and Peacock, A. C. 1973. Differential staining of phosphoproteins on polyacrylamide gels with a cationic carbocyanine dye. Analytical Biochemistry. 56: 43-51.

Han, D., Kim, D., Choi, S. and Yoh, J. J. 2017. A novel classification of polymorphs using combined libs and raman spectroscopy. Current Optics and Photonics. 1: 402-411.

Huang, J., Liu, C., Xie, L. and Zhang, R. 2018. Amorphous calcium carbonate: A precursor phase for aragonite in shell disease of the pearl oyster. Biochemical and Biophysical Research Communications. 497: 102-107.

Kocot, K. M., Aguilera, F., McDougall, C., Jackson, D. J. and Degnan, B. M. 2016. Sea shell diversity and rapidly evolving secretomes: Insights into the evolution of biomineralization. Frontiers in Zoology. 13: 23.

Kong, J., Liu, C., Yang, D., Yan, D., Chen, Y., Liu, Y., Zheng, G., Xie, L. and Zhang, R. 2019. A novel basic matrix protein of *Pinctada fucata*, pnu9, functions as inhibitor during crystallization of aragonite. CrystEngComm. 21: 1250-1261.

Kong, Y., Jing, G., Yan, Z., Li, C., Gong, N., Zhu, F., Li, D., Zhang, Y., Zheng, G., Wang, H., Xie, L. and Zhang, R. 2009. Cloning and characterization of prisilkin-39, a novel matrix protein serving a dual role in the prismatic layer formation from the oyster *Pinctada fucata*. Journal of Biological Chemistry. 284: 10841-10854.

Laemmli, U. K. 1970. Cleavage of structural poteins during the assembly of the head of bacteriophage t4. Nature. 227: 680-685.

Levi-Kalisman, Y., Falini, G., Addadi, L. and Weiner, S. 2001. Structure of the nacreous organic matrix of a bivalve mollusk shell examined in the hydrated state using cryo-tem. Journal of Structural Biology. 135: 8-17.

Liang, J., Xie, J., Gao, J., Xu, C.-Q., Yan, Y., Jia, G.-C., Xiang, L., Xie, L.-P. and Zhang, R.-Q. 2016. Identification and characterization of the lysine-rich matrix protein family in *Pinctada fucata*: Indicative of roles in shell formation. Marine Biotechnology. 18: 645-658.

Loste, E., Wilson, R., Seshadri, R. and Meldrum, F. C. 2003. The role of magnesium in stabilising amorphous calcium carbonate and controlling calcite morphologies. Journal of Crystal Growth. 254: 206-218.

Ma, Y. and Feng, Q. 2015. A crucial process: Organic matrix and magnesium ion control of amorphous calcium carbonate crystallization on b-chitin film. CrystEngComm. 17: 32-39.

Meldrum, F. C. and Colfen, H. 2008. Controlling mineral morphologies and structures in biological and synthetic systems. Chemical Reviews. 108: 4332-4432.

Montagnani, C., Marie, B., Marin, F., Belliard, C., Riquet, F., Tayalé, A., Zanella-Cleon, I., Fleury, E., Gueguen, Y., Piquemal, D. and Cochennec-Laureau, N. 2011. Pmarg-pearlin is a matrix protein involved in nacre framework formation in the pearl oyster *Pinctada margaritifera*. ChemBioChem. 12: 2033-2043.

Nassif, N., Pinna, N., Gehrke, N., Antonietti, M., Jager, C. and Colfen, H. 2005. Amorphous layer around aragonite platelets in nacre. Proceedings of the National Academy of Sciences of the United States of America. 102: 12653-12655.

Nielsen, M. R., Sand, K. K., Rodriguez-Blanco, J. D., Bovet, N., Generosi, J., Dalby, K. N. and Stipp, S. L. S. 2016. Inhibition of calcite growth: Combined effects of Mg^{2+} and SO_4^{2-}. Crystal Growth & Design. 16: 6199-6207.

Pan, C., Fang, D., Xu, G., Liang, J., Zhang, G., Wang, H., Xie, L. and Zhang, R. 2014. A novel acidic matrix protein, pfn44, stabilizes magnesium calcite to inhibit the crystallization of aragonite. Journal of Biological Chemistry. 289: 2776-2787.

Politi, Y., Metzler, R. A., Abrecht, M., Gilbert, B., Wilt, F. H., Sagi, I., Addadi, L., Weiner, S. and Gilbert, P. U. P. A. 2008. Transformation mechanism of amorphous calcium carbonate into calcite in the sea urchin larval spicule. Proceedings of the National Academy of Sciences of the United States of America. 105: 17362-17366.

Radha, A. V., Forbes, T. Z., Killian, C. E., Gilbert, P. U. P. A. and Navrotsky, A. 2010. Transformation and crystallization energetics of synthetic and biogenic amorphous calcium carbonate. Proceedings of the National Academy of Sciences of the United States of America. 107: 16438-16443.

Raz, S., Weiner, S. and Addadi, L. 2000. Formation of high-magnesian calcites via an amorphous precursor phase: Possible biological implications. Advanced Materials. 12: 38-42.

Rousseau, M., Meibom, A., Geze, M., Bourrat, X., Angellier, M. and Lopez, E. 2009. Dynamics of sheet nacre formation in bivalves. Journal of Structural Biology. 165: 190-195.

Soldati, A. L., Jacob, D. E., Wehrmeister, W. and Hofmeister, W. 2008. Structural characterization and chemical composition of aragonite and vaterite in freshawater cultured pearls. Mineralogical Magazine. 72: 579-592.

Song, X., Liu, Z., Wang, L. and Song, L. 2019. Recent advances of shell matrix proteins and cellular orchestration in marine molluscan shell biomineralization. Frontiers in Marine Science. 6.

Song, X., Wang, X., Li, L. and Zhang, G. 2014. Identification two novel nacrein-like proteins involved in the shell formation of the pacific oyster *Crassostrea gigas*. Molecular Biology Reports. 41: 4273-4278.

Suzuki, M., Murayama, E., Inoue, H., Ozaki, N., Tohse, H., Kogure, T. and vNagasawa, H. 2004. Characterization of prismalin-14, a novel matrix protein from the prismatic layer of the japanese pearl oyster (*Pinctada fucata*). Biochemical Journal. 382: 205-213.

Tobler, D. J., Rodriguez-Blanco, J. D., Dideriksen, K., Bovet, N., Sand, K. K. and Stipp, S. L. S. 2015. Citrate effects on amorphous calcium carbonate (acc) structure, stability, and crystallization. Advanced Functional Materials. 25: 3081-3090.

Weiss, I. M., Kaufmann, S., Mann, K. and Fritz, M. 2000. Purification and characterization of perlucin and perlustrin, two new proteins from the shell of the mollusc *Haliotis laevigata*. Biochemical and Biophysical Research Communications. 267: 17-21.

Wilt, F. H. 2005. Developmental biology meets materials science: Morphogenesis of biomineralized structures. Developmental Biology. 280: 15-25.

Wolf, S., Marin, F., Marie, B., Hamada, S. B., Silva, P., Montagnani, C., Joubert, C., Piquemal, D. and Le Roy, N. 2013. Shellome: Proteins involved in mollusc shell biomineralization - diversity, functions. In: S. Watabe, K. Maeyama and H. Nagasawa, editors. Recents advances in pearl research: Terrapub. pp. 149-166.

Xie, J., Liang, J., Sun, J., Gao, J., Zhang, S., Liu, Y., Xie, L. and Zhang, R. 2016. Influence of the extrapallial fluid of *Pinctada fucata* on the crystalization of calcium carbonate and shell biomineralization. Crystal Growth & Design. 16: 672-680.

Xu, N., Li, Y., Zheng, L., Gai, Y., Yin, H., Zhao, J., Chen, Z., Chen, J. and Chen, M. 2014. Synthesis and application of magnesium amorphous calcium carbonate for removal of high concentration of phosphate. Chemical Engineering Journal. 251: 102-110.